

Two-dimensional Topology-Seeded Graphitization for Highly Thermally Conductive Carbon Fibers

Xing Ming¹, Anran Wei², Yingjun Liu^{1,3*}, Li Peng¹, Peng Li¹, Jiaqing Wang¹, Sengping Liu¹, Wenzhang Fang¹, Ziqiu Wang¹, Huanqin Peng¹, Jiahao Lin¹, Haoguang Huang¹, Zhanpo Han¹, Shiyu Luo¹, Min Cao¹, Bo Wang¹, Zheng Liu⁴, Fenglin Guo^{2*}, Zhen Xu^{1*}, Chao Gao^{1*}

¹MOE Key Laboratory of Macromolecular Synthesis and Functionalization, Department of Polymer Science and Engineering, Key Laboratory of Adsorption and Separation Materials & Technologies of Zhejiang Province, Zhejiang University, 38 Zheda Road, Hangzhou 310027, China.

²School of Naval Architecture, Ocean and Civil Engineering (State Key Laboratory of Ocean Engineering), Shanghai Jiao Tong University, Shanghai 200240, China.

³Shanxi-Zheda Institute of Advanced Materials and Chemical Engineering, Taiyuan, China

⁴Jiangsu Province Special Equipment Safety Supervision and Inspection Institute, National Graphene Products Quality Inspection and Testing Center, 330 Yanxi Road, Wuxi 214174, China.

*Corresponding author. Email: yingjunliu@zju.edu.cn (Y. L.); flguo@sjtu.edu.cn (F. G.); zhenxu@zju.edu.cn (Z. X.); chaogao@zju.edu.cn (C. G.).

Keywords: highly thermally conductive, carbon fiber, topology-graphitization, 2D seed, graphene oxide

Abstract

Highly thermally conductive carbon fibers (CFs) have become an important material to meet the increasing demand for efficient heat dissipation. To date, the high thermal conductivity has been only achieved in the specific Pitch-based CFs with high crystallinity. However, obtaining high graphitic crystallinity and high thermal conductivity beyond Pitch-CFs remains a grand challenge. Here, we present a 2D topology-seeded graphitization method to mediate the topological incompatibility in graphitization by seeding 2D graphene oxide (GO) sheets into the polyacrylonitrile (PAN) precursor. Strong mechanical strength and high thermal conductivity up to 850 W/mK are simultaneously realized, which are one order of magnitude higher in conductivity than commercial PAN-based CFs. The self-oxidation and seeded graphitization effect generate large crystallite size and high orientation

This article has been accepted for publication and undergone full peer review but has not been through the copyediting, typesetting, pagination and proofreading process, which may lead to differences between this version and the [Version of Record](#). Please cite this article as [doi: 10.1002/adma.202201867](https://doi.org/10.1002/adma.202201867).

This article is protected by copyright. All rights reserved.

to far exceed those of conventional CFs. Topologically seeded graphitization, verified in experiments and simulations, allows converting the non-graphitizable into graphitizable materials by incorporating 2D seeds. This method extends the preparation of highly thermally conductive CFs, which has great potential for lightweight thermal management materials.

1. Introduction

The demand for highly thermally conductive materials is rapidly increasing in the electronic and aerospace industries owing to the boosted level of heat dissipation^[1]. Highly thermally conductive CFs have many advantages such as lightweight, high strength, excellent conductivity, and low thermal expansion coefficient in a wide temperature range^[2]. CFs can not only be used as efficient thermal management materials to maintain the functionality and reliability of microelectronic components with high heat flux, but also be used as high-performance composites for thermal protection of flight devices in the aerospace field^[3]. In spite of their wide uses, the specific Pitch-based CFs are the only commercial species of highly thermally conductive CFs with high cost^[4]. As a comparison, the other commercial PAN-based CFs have strong mechanical properties but poor thermal conductivity due to their limited graphitic crystallinity, determining their confined application as lightweight structural materials^[2a, 5]. In this context, it is necessary to expand alternative sources of highly thermally conductive fibers beyond the sole Pitch-based CFs^[2b, 6]. An intuitive option is translating PAN-based CFs to highly thermally conductive species, but remains a forbidden task that is challenged by the intrinsic incompatibility between the 1D topology of linear polymers and the 2D topology of target graphitic crystallinity^[5b, 7].

The thermal conductivity of graphitic materials is determined by their complicated nano textures and spans a wide range from ~ 6 W/mK in glassy carbon to ~ 2000 W/mK in pyrolytic graphite at room temperature^[8]. In principle, the perfect crystalline textures in graphitic materials ensure efficient phonon transport and high thermal conductivity^[8]. As a result, larger crystallite size, higher crystallites orientation, and lower defect density facilitate the achievement of high thermal conductivity, such as the ideal single crystal of graphite whiskers with thermal conductivity up to 2000 W/mK^[3b]. For the commercial PAN-based CFs, the interior graphite crystals are formed through an interphase cluster process at high temperatures and far deviate from the perfection of graphite whiskers^[9]. Specifically, the 1D linear PAN chains are firstly merged to form Oberlin's Local Molecular Orientation clusters (LMOs) via oxidation and pyrolysis^[10]. Whereas, the translational and rotational activation energies of LMOs transformed from polymeric chains with low flatness are too high in the subsequent flattening process, which makes it difficult to adjust the grain distributions from chaotic arrangement to ideal 2D crystal stacking even after 3000 °C annealing. This mechanism reflects the intrinsic incompatibility between the 1D topology of polymer precursors and 2D target graphitic

crystallinity^[7b]. For this incompatibility, the high dynamic barrier in the PAN case defies the elimination of topological defects and voids in the LMOs and causes tiny graphite crystals (smaller than 8 nm) with crosslinking textures^[5b]. The immature crystallinity of PAN-based CFs results in massive phonon scattering centers to depress phonon transport and the inferior thermal conductivity (32 W/mK), lowering to Pitch-based CFs (600-1000 W/mK) and ideal graphite whiskers^[3b, 8].

In the pursuit of enhancing the functionality of PAN-based CFs, several methods have been tried to optimize their graphitic crystallinity. Multistage stretching is widely used in industry to obtain highly orientated precursors^[2a]. Due to the unavoidable thermal relaxation and low graphitizability of PAN, the final graphitic crystallites are still limited to several nanometers. The second is doping heterogeneous elements (such as boron element) to catalyze the graphitization and modify the kinetic process, in order to achieve higher crystallinity at lower temperature with less economic cost^[11]. Whereas, the residual heteroatoms would reduce the thermal conductivity of CFs. The third is adding a small amount of nano-sized graphene sheets or CNTs^[12]. Following this procedure, the mechanical properties are reinforced by reducing voids of CFs, however, continuous confined topology networks are still unable to form in the polymer matrix, which results in unsatisfied improvement of thermal conductivity after graphitization. These attempts have not fundamentally improved the size and orientation of graphitic crystalline in PAN-based CFs^[2c]. To date, how to effectively modulate the topology mismatch between 1D linear polymeric chains and desired 2D graphite crystallite has remained a great challenge and PAN-based CFs are still extremely weak in thermal conductivity^[7b, 8, 13].

Here, we adopt a 2D topology-seeded strategy to regulate the graphitization process of PAN linear polymer to produce highly thermally conductive and strong CFs with preferred 2D graphitic crystallinity. By incorporating large-size GO sheets as 2D topological seeds, the topology mismatch between 1D linear precursors and 2D graphitic basal planes are effectively alleviated to promote the growth of graphitic crystallites. The prepared PAN/GO fibers (PGF) finally possess superior thermal conductivity (~ 850 W/mK), highly electrical conductivity ($\sim 3.5 \times 10^5$ S/m), and strong mechanical strength (~ 2.4 GPa). Our 2D topology-seeded graphitization strategy effectively endows the PAN-based CFs with high thermal conductivity. Moreover, the 2D topology-seeded graphitization methodology possibly becomes a general method to guide the structural design, production and applications of graphitic materials.

2. Result and discussion

2.1. High-performance carbon fibers via 2D topology-seeded graphitization strategy

The current preparation of graphitic fibers relies on pyrolyzing 1D linear polymeric precursors (such as PAN, lignin and cellulose) (Figure 1a)^[2a, 2c, 3b]. In the popular PAN-based CFs case, the interior graphitic crystal textures usually consist of tiny graphite crystalline grains (lateral size $\langle L \rangle$ smaller than 8 nm)^[2a, 5c], which are interconnected with amorphous carbon structures, as shown in high-resolution transmission electron microscopy (HR-TEM) images in Figure 1a. According to the interphase theory of graphitization, 1D linear PAN chains firstly undergo polycondensation reactions to form LMOs composed of ladder polymers during oxidation and low-temperature carbonization. Then, LMOs are fused together via bonding adjacent edges above a critical high-temperature threshold to form tiny graphite interphase grains^[9-10]. Until the graphitization end, the translational and rotational activation energies of LMOs and intermediate grains are usually too high to achieve uniform orientation for generating large 2D graphitic crystal units^[7b], which inevitably leads to the misfused graphitic basal planes in the PAN-derived CFs^[7a]. These disordered crystal structures generate high mechanical strength, but poor thermal conductivity (~ 32 W/mK)^[5c]. Therefore, enhancing the thermal conductivity of PAN-CFs is dependent on perfecting the internal graphitic crystal structure, which has become an unsolved challenge for decades^[2c].

We propose a 2D topology-seeded graphitization strategy to boost the weak thermal conductivity of PAN-CFs to the level of the benchmark Pitch-based CFs. Our topology-seeded principle reconciles the intrinsic dimension mismatch between 1D linear polymers and 2D graphitic basal planes (Figure 1b). The large-size GO sheets with single-layer thickness are selected as 2D topological crystal seeds, and PAN/GO precursor fibers (p-PGOF) are fabricated by single-filament liquid crystal wet-spinning. (Figure S1 and S2, Supporting Information)^[6b, 14]. Besides, the pure PAN precursor fibers (p-PF) are also prepared through the same process. The introduction of 2D GO seeds promotes the graphitization process of 1D linear PAN molecules and achieves high graphitic crystallinity after thermal treatments (Figure 1b). The obtained p-PGOF are firstly conducted oxidation process and then annealed at 1000 °C, 2000 °C and 3000 °C to prepare corresponding carbonized fibers and graphite fibers. We boost the lateral size of graphitic grains to 430 nm by one order of magnitude, as compared with neat graphited PAN fibers (g-PF)^[5b, 5c]. The graphited PAN/GO fibers (g-PGF) exhibits thermal conductivity as high as 850 W/mK, far overwhelming conventional PAN-based CFs and approaching 950 W/mK of benchmark meso-phase Pitch-CFs (K1100) (Figure

1c)^[2c, 4a]. Following the 2D topology-seeded graphitization, we exploit the other trend of commercial PAN-based CFs as high crystalline graphite fibers with outstanding thermal conductivity, breaking the functional limitations of commercial PAN-based carbon and graphite fibers^[5b] (Figure 1d). The topology-seeded graphitization strategy provides a novel insight to regulate the graphitization process of polymers.

2.2. Crystal structures and conductive properties of PGF with varied seed concentrations

We wet-spin p-PGF and obtained 2D seeded graphite fibers (i.e. g-PGF) with varied seed concentrations after thermal treatment up to 3000 °C. The evolution of defects and crystallinity of g-PGF is monitored as seed concentration increases. The homogeneously mixed GO sheets act as 2D seeds to guide the perfection of graphitic crystallinity. It is found increasing 2D topology-seeded density promotes higher crystallinity and larger grain size.

Raman spectra of g-PF and g-PGF are obtained under ambient condition using an excitation wavelength of 532 nm laser beam (Figure 2a). It is shown that the intensity of D peak (1350 cm^{-1}) of g-PGF is dramatically weakened as the seed concentrations increase. Meanwhile, the integrated intensity ratio of D to G peak (I_D/I_G) gradually decreases from 0.29 (g-PF) to 0.024 (g-PGF-30%) (Figure S3, Supporting Information), indicating the effective restoration of defect-free graphitic structures by seeded graphitization^[2b, 15]. Accordingly, the lateral length (L_a) of graphitic crystallites is immensely promoted to 485 nm (g-PGF-30%), 740% larger than that of nascent g-PF (Figure 2c). In addition, the incremental 2D seeded growth of graphitic crystals significantly enhances the alignment of basic graphitic planes to achieve the AB stacking configuration, as demonstrated by the evolution of the 2D band from a single broad peak to two peaks with an enhanced intensity of 2D₂ shoulder peak (2720 cm^{-1}) (Figure 2a)^[16]. The 2θ value of (002) peak in the XRD patterns of g-PGF shifts from 26.3° (g-PF) to 26.5° (g-PGF-30%) with the corresponding full width at half maximum (FWHM) narrowing from 0.92° to 0.18° , demonstrating a higher crystallinity of g-PGF with increasing 2D seed concentrations (Figure 2b)^[2b, 15a]. The crystallite thickness (L_c) of g-PGF is promoted from 9.8 nm of g-PF to 48 nm of g-PGF-30%, meanwhile, the graphitization degree monotonically boosts from 66.9% to 94.7% (Figure 2c and Table S4, Supporting Information). The enlarged crystallites size and graphitization degree are mainly ascribed to the compact and aligned microstructures induced by 2D seeded graphitization.

In contrast to the reinforced efficiency of 1D CNT or nano-size graphene, large-size GO sheets exhibit a more effective seeded effect for topology adaptation of desired 2D graphitic

structures, resulting continuous 2D topology networks with broader interaction surface and tighter connection^[12a-c]. The 2D seeded graphitization endows the melioration of graphitic crystal structures in g-PGF to achieve extraordinary electrical and thermal conductivity. The highest thermal and electrical conductivities of g-PGF-30% reach 850 W/mK and 3.5×10^5 S/m, surpassing those of g-PF (126 W/mK and 0.5×10^5 S/m), and already reaching the conductive level of Pitch-based CFs (Figure 2d, 2e and Table S3, Supporting Information). Beyond a threshold of seed concentration (30%), a slight decline in conductive performance occurs for the structural deterioration of the corresponding precursor fibers^[17]. The thermal and electrical conductivities of g-PGF-50% still maintain at 770 W/mK and 3.2×10^5 S/m, about 6 times higher than those of g-PF. The improved conductivity of g-PGF directly indicates that 2D seeds greatly regulate the graphitization kinetics of 1D linear polymer to realize high crystal parameters and crystallinity^[7b, 8].

2.3. Self-oxidation effect of 2D seeds at low-temperature

In the nascent fibers, the 1D linear PAN chains are constrained and aligned between the interlayer of 2D GO sheets by forming a critical interphase (Figure S4, Supporting Information)^[17-18]. Verified by the differential scanning calorimetry (DSC) curves, the glass transition temperature (T_g) exhibits a strong increment from 56 °C of p-PF to 97 °C of p-PGOF (30% GO seeds) (Figure S5, Supporting Information). The increase of T_g is caused by the enhanced surface interactions between the 1D polymer and 2D GO seeds, which suppresses the mobility of polymeric chains to generate dense and ordered structures of p-PGOF (Figure S6, Supporting Information)^[17b, 18-19]. The strong binding of PAN chains guarantees the subsequent topology transformation during thermal treatment.

Improving compositional uniformity in the radial direction is generally beneficial to prepare high-performance fibers. The obtained p-PF and p-PGOF are firstly conducted oxidation process at 250 °C for 2 h in the air atmosphere to get the oxidized PAN fibers (o-PF) and oxidized PAN/GO fibers (o-PGF) (See Supporting Information for more details)^[20]. In the low-temperature oxidation process, the o-PF has a skin-core structure due to the decreased diffusion rate of oxygen atoms^[21]. This ununiform microstructure is inevitably retained in the g-PF, resulting in their decayed properties. Impressively, 2D GO seeds serve as an additional source of oxygen through a self-oxidation effect, due to their abundant oxygen-containing functional groups (Figure S7, Supporting Information)^[12d, 22]. Time-of-flight secondary ion mass spectrometry (ToF-SIMS) measurements are conducted to measure

the distribution of oxygen element in the radial direction of o-PF and o-PGF. The intensity of oxygen element of o-PGF keeps stable at 0.88 while rapidly declines from surface (0.87) to core (0.12) in o-PF (Figure 3a). The effective elimination of inhomogeneity of oxygen distribution in the fibers is observed from the 2D surface and 3D bulk phase (Figure 3b and 3c). However, excess GO seeds cause structural degradation of PGF due to the oxidation of GO in the air. The residual weight of p-PGOF-30% is the highest (84.6%) among the p-PF (80.7%), p-PGOF-70% (60.1%), and p-GOF (43.7%) after oxidation in the air (Figure S8 and Table S1, Supporting Information).

2.4. 2D topology-seeded crystal growth at high temperature

To look into the 2D topology-seeded crystal growth during high-temperature treatments, we track the structural evolution of p-PGOF (30% GO seeds). An obvious D peak (1350 cm^{-1}) in the Raman spectra of PF appears with the increasement of annealing temperature up to $3000\text{ }^{\circ}\text{C}$, denoting the poor graphitization process of 1D linear polymers (Figure S9, Supporting Information). Conversely, the 2D seeds significantly and persistently promote the graphitization of 1D linear polymers to form long-range ordered graphitic structures, which are difficult to form during thermal treatments of traditional PAN-CFs. Calculated from the Raman spectra, the size of graphite domains of PGF rapidly boosts from 127 nm ($1000\text{ }^{\circ}\text{C}$) to 485 nm ($3000\text{ }^{\circ}\text{C}$) while restricted under 65 nm in PF (Figure S10, Supporting Information). The enlarged crystalline domains of g-PGF are coherently verified by HR-TEM characterizations. The (002) facet orientation in the selected area electron diffraction (SAED) of a single fiber axial slice of PGF gradually sharpens but keeps a dispersed ring in PFs (Figure S11 and S12, Supporting Information). Distinct from strong lattice distortion and defects in g-PF, the crystallites of g-PGF are homogeneously aligned along the fiber axis with L_a of over 100 nm and L_c of 15 nm , which are observed in corresponding HR-TEM images (Figure 3d and 3e).

Profited from the preferred orientation growth of crystallites by 2D seeds, the wide-angle X-ray scattering (WAXS) pattern of g-PGF presents an obviously crescent (100) and (101) peaks. The (002) peak possesses a higher Herman's orientation factor of 0.83 in g-PGF than 0.68 in g-PF (Figure 3f, 3g and Figure S13, Supporting Information)^[6b, 14, 23]. Azimuthal scanning of equatorial scattering pattern in small-angle X-ray scattering (SAXS) consistently displays an order parameter of 0.80 for g-PGF, much higher than that of g-PF without 2D seeds (0.63; Figure 3h and 3i)^[6b, 14, 23-24]. The crystallization kinetics of 2D topology-seeded growth is continuously promoted by reducing the energy barrier with the increased sp^2 conjugated structures during heat treatment. (Figure S14, Supporting Information)^[9-10]. As a

Accepted Article

result, the final 2D seeded PGF maintains the largest crystallite sizes to 485 nm, contrasted with the commercial graphitized PAN-based CFs (15 nm) and Pitch-based CFs (22 nm, Figure 3j)^[5b]. Besides, we further calculate the La size of g-PGF (30% GO seeds) by radical scanning at the q_y direction in the WAXS image (Figure 3g). The La of g-PGF is also extremely larger than that of the best commercial PAN-based CFs and Pitch-based CFs (Figure S29). Meanwhile, the O and N heteroatoms of PGF are nearly removed after seeded graphitization when annealed at 2000 °C as compared with the PF (Figure S15 and S16, Supporting Information). The PGF also exhibits a higher residual weight (49.58%) than that of PF (31.75%) (Figure S17, Supporting Information).

The overall higher crystalline order and giant crystalline size of 2D seeded PGF jointly lead to an integration of both exceptional conductive and mechanical properties, overwhelming PAN-based CFs^[2a, 5c]. A modified steady-state electrical heating method is conducted to measure the thermal conductivity of thin PGF (Figure S18, Supporting Information)^[2b, 23b, 25]. The thermal and electrical conductivities of the PGF (30% GO seeds) raise sharply with the annealing temperature for reducing phonon/electron scattering centers, which greatly exceed conventional PAN-based CFs by nearly one order of magnitude. The highest thermal conductivity and electrical conductivity of g-PGF measured are 850 W/mK and 3.5×10^5 S/m, respectively, surpassing those of g-PF (126 W/mK and 0.5×10^5 S/m) (Figure 3k and Figure S19, Supporting Information). Moreover, the PGF single filaments possess an average tensile strength of 2.4 GPa, which is 5.6 times than that of PF (0.45 GPa) (Figure 3l, Figure S20 and Table S2, Supporting Information). The strong mechanical performances are attributed to the optimized crystal alignments, growing crystal sizes of c-PGF and partially residual covalent crosslinks between neighboring graphitic domains^[2a, 2b, 13]. It needs to be noted that the stretching ratio of g-PF is far less than that of conventional CFs in industrial production, resulting in its mechanical strength being still lower than that of traditional CFs (Figure 1c, Figure 3l and Table S6, Supporting Information).

2.5. Mechanism of 2D topology-seeded graphitization

We adopt a sandwich-like PAN/GO/PAN (PGP) composite nanofilms as an element model to elucidate the induction depth of 2D seeds. The self-standing carbonized PGP nanofilm with a thickness of 30 nm graphene nanofilm is prepared by the stepwise assembly and thermal annealing (Figure S21 and S22, Supporting Information)^[16a]. From the cross-sectional HR-TEM inspection and corresponding fast Fourier transform (FFT) spectra, a lattice transition region significantly develops

with (002) facet orientation, which is parallel with the original graphene layers (Figure 4a). The average depth statistics of the transition region firstly indicate that 2D seeds promote the alignment of 1D linear polymers with 5 atomic layers near the vicinity of graphene (Figure 4b). With 2D topology-seeded graphitization, the atomic texture of 1D PAN chains is effectively transformed from amorphous carbon to 2D ordered graphitic crystalline, which has been quantitatively described.

We further perform Atomistic ReaxFF MD simulations to thoroughly investigate the evolution mechanism of 2D topology-seeded graphitization^[12a, 26]. Both pure PF and 2D seeded p-PGOF systems are established to track the evolutions of pyrolysis products, chemical constitution, and structural configurations during heat treatments (Figure 4c). At the low-temperature oxidation stage, the p-PGOF system shows an improved molecular fusion, the production of 6-membered carbon rings is 1.34 times higher than that of pure PF (Figure S23, Supporting Information), which verifies the aforementioned self-oxidation effect. Subsequently, the snapshots of structural configurations of two systems at 2800 K indicate that the g-PGF system with 2D topology-seeded graphitization, which reveals an obviously faster trend of facet orientation and crystallite sizes (Figure S24, Supporting Information). The simulation results demonstrate that the proportion of 6-membered carbon rings in the PGF system is higher than that of the PF system over time, and the proportion of 5/7-membered carbon rings is lower (Figure S25, Supporting Information). Meanwhile, contrasted with the slight production of CO and CO₂ in the PF system, no carbonaceous products are generated in the PGF system for ensuring higher carbon residue (Figure S26 and S27, Supporting Information), which is consistent with previous TGA results. Benefiting from the unique 2D topology and active defect chemistry of GO seeds^[12d, 20a, 22], the newly generated 6-membered carbon rings are more likely to be connected with the edge defects of 2D GO seeds and have a distinct preferred orientation angle ($\cos\alpha=0.8$), which is parallel to the initial seed (Figure 4d and 4e). The average Herman's orientation parameter of graphite crystallites in the PGF system up to 0.26 is 3.6 times higher than that of the PF system (0.06, Figure 4f).

As a result, during the 2D topology-seeded graphitization, the density of aligned 1D polymer chains which is directly adjacent to GO seeds is the highest to facilitate the formation of orientated LMOs at the early fusion stage, laying a kinetic predominance for growing of the graphitic crystals^[7b, 12a, 19, 27]. At the subsequent graphitization stage, the 2D GO seeds possess a lower energy barrier to induce and interconnect with LMOs for growing rapidly through the in-plane (L_a) and out-plane (L_c) directions, finally achieving a large size of graphite crystallites (Figure 4g).

2.6. Comprehensive comparison of PGF with 2D topology-seeded graphitization

The internal crystal structure of fibers determines their physical properties^[2a]. For traditional PAN-CFs, their internal graphitic crystallites are tiny and mismatched with strong interlayer crosslinking^[5b], causing low thermal/electrical conductivity^[5c]. The favorable tailoring crystal orientation and size have been realized by introducing the highly oriented 2D GO seeds, which are superior to the conventional PAN-CFs (Figure S28, Supporting Information). The PGF with 2D seeded graphitization exhibits overwhelmingly high strength (2.4 GPa), which breaks through the limit of previous composite fibers (Figure 5c and Table S5, Supporting Information). However, the mechanical properties of PGF are lower than that of conventional CFs in industrial production due their intrinsically different spinning process (Table S6, Supporting Information). From a functional view of CFs, the PGF enormously boosts the thermal conductivity of commercial PAN-based CFs by 4.6 times to reach the level of Pitch-based CFs (Figure 5d and Table S7, Supporting Information). Notably, the ultimate specific thermal conductivity of the obtained g-PGF surpasses most previously reported fibers, including metal fibers, PAN-based CFs and Pitch-based CFs, and is even comparable to the best K1100 fibers, which features a specific thermal conductivity of $450 \text{ mW}\cdot\text{m}^2/\text{kg}\cdot\text{K}$ with a density of $1.9 \text{ g}/\text{cm}^3$ (Figure 5e and Table S8, Supporting Information)^[1c, 4a]. These results indicate the as-prepared strong PGF holds higher thermal conductivity, exhibit the great potential to break the limit of Pitch CFs and relieve the urgently thermal management demands^[3a].

3. Conclusion

In summary, we demonstrate a 2D topology-seeded graphitization strategy to obtain a new specie of highly thermally conductive CFs from the PAN precursor. The introduction of 2D GO seeds successfully mediates the topology mismatch between 1D linear polymers and 2D graphitic crystallites. The 2D seeds effectively endow uniform structures and promote graphitization kinetics of non-graphitized polymers for facilitating the 2D preferred growth of graphitic crystallites. Experiments and theoretical analysis jointly reveal the mechanism of 2D seeded graphitization via reducing energy barrier to induce and interconnect with LMOs of polymers for rapidly enlarging graphite crystallites and improving crystalline orientation. The 2D seeded PAN fibers after high-temperature treatments exhibit a record thermal conductivity (850 W/mK) and strong tensile strength (2.4 GPa). The specific thermal conductivity of seeded fibers ($450 \text{ mW}\cdot\text{m}^2/\text{kg}\cdot\text{K}$) surpasses most previous fibers, including metal fibers and traditional PAN-CFs and Pitch-CFs. Our work clarifies

the topological transformation principle of 2D seeded graphitization, guides the preparation of highly thermally conductive fibers from 1D polymers and promotes more applications of functional fibers in lightweight engineering material, high-power electronics, and energy storage.

4. Experimental Section

Methods and any associated references are available in the Supporting Information.

Supporting Information

Supporting Information is available from the Wiley Online Library or from the author.

Acknowledgements

We thank the members of staffs at Shanghai Synchrotron Radiation Facility (SSRF) for assistance in SAXS and WAXS characterizations. This work is supported by the National Natural Science Foundation of China (Nos. 52090030, 51973191, 52122301), the Fundamental Research Funds for the Central Universities (No. 2021FZZX001-17), Hundred Talents Program of Zhejiang University (188020*194231701/113), Key Laboratory of Novel Adsorption and Separation Materials and Application Technology of Zhejiang Province (512301-I21502), China Postdoctoral Science Foundation (2020M681819), the Research Fund for Nanjing University of Aeronautics and Astronautics (INMD-2021M06) and Shanxi-Zheda Institute of New Materials and Chemical Engineering (2012SZ-FR004).

Conflict of Interest

The authors declare no conflict of interest.

Author Contributions

X. M., Y.J. L., Z. X. and C. G. conceived and designed the research. A.R. W. and F.L. G. performed the simulation experiments. X. M. and P. L. prepared the fibers, X. M., Z.Q. W. and B. W performed the experiments on the graphitization of the fibers. X. M. and L. P. prepared the composite nanofilms. X. M. and W.Z. F. performed the experiments on the graphitization of composite nanofilms. X. M. and H.Q. P. conducted the Raman and XRD tests. X. M., P. L., J.Q. W. and Z.P. H. performed the tensile tests of fibers. X. M. and S.P. L. performed the TEM and SEM characterizations. X. M. and H.Q. P. performed the WAXS and SAXS tests of fibers. X. M., J.H. L., S.Y. L. and Z. L. performed the tests of thermal conductivity. X. M., H. G. H., M. C. and Z. L. performed the tests of electrical conductivity.

Data Availability Statement

The data that support the finding of this study are available from the corresponding author upon reasonable request.

Received: ((will be filled in by the editorial staff))

Revised: ((will be filled in by the editorial staff))

Published online: ((will be filled in by the editorial staff))

References

- [1] a) Y. Li, W. Li, T. Han, X. Zheng, J. Li, B. Li, S. Fan, C.-W. Qiu, *Nat. Rev. Mater.* **2021**, *6*, 488; b) H. Song, J. Liu, B. Liu, J. Wu, H.-M. Cheng, F. Kang, *Joule* **2018**, *2*, 442; c) N. Behabtu, C. C. Young, D. E. Tsentelovich, O. Kleinerman, X. Wang, A. W. K. Ma, E. A. Bengio, R. F. Ter Waarbeek, J. J. De Jong, R. E. Hoogerwerf, S. B. Fairchild, J. B. Ferguson, B. Maruyama, J. Kono, Y. Talmon, Y. Cohen, M. J. Otto, M. Pasquali, *Science* **2013**, *339*, 182.
- [2] a) E. Frank, L. M. Steudle, D. Ingildeev, J. M. Spörl, M. R. Buchmeiser, *Angew. Chem. Int. Ed.* **2014**, *53*, 5262; b) G. Xin, T. Yao, H. Sun, S. M. Scott, D. Shao, G. Wang, J. Lian, *Science* **2015**, *349*, 1083; c) W. J. A. M. Ruland, *Adv. Mater.* **1990**, *2*, 528.
- [3] a) W. Feng, M. Qin, Y. Feng, *Carbon* **2016**, *109*, 575; b) P. Morgan, *Carbon fibers and their composites*, CRC press, **2005**.
- [4] a) F. G. Emmerich, *Carbon* **2014**, *79*, 274; b) P. M. Adams, H. A. Katzman, G. S. Rellick, G. W. Stupian, *Carbon* **1998**, *36*, 233.
- [5] a) K. Naito, Y. Tanaka, J.-M. Yang, Y. Kagawa, *Carbon* **2008**, *46*, 189; b) X. Qin, Y. Lu, H. Xiao, Y. Wen, T. Yu, *Carbon* **2012**, *50*, 4459; c) H. A. Katzman, P. M. Adams, T. D. Le, C. S. Hemminger, *Carbon* **1994**, *32*, 379.
- [6] a) Z. Xu, C. Gao, *Materials Today* **2015**, *18*, 480; b) P. Li, Y. Liu, S. Shi, Z. Xu, W. Ma, Z. Wang, S. Liu, C. Gao, *Adv. Funct. Mater.* **2020**, *30*, 2006584.
- [7] a) N. Gupta, V. I. Artyukhov, E. S. Penev, B. I. Yakobson, *Adv. Mater.* **2016**, *28*, 10317; b) P. Ouzilleau, A. E. Gheribi, P. Chartrand, G. Soucy, M. Monthieux, *Carbon* **2019**, *149*, 419; c) M. Kopeć, M. Lamson, R. Yuan, C. Tang, M. Kruk, M. Zhong, K. Matyjaszewski, T. Kowalewski, *Prog. Polym. Sci.* **2019**, *92*, 89.
- [8] A. A. Balandin, *Nat. Mater.* **2011**, *10*, 569.
- [9] P. Ouzilleau, A. E. Gheribi, P. Chartrand, *Carbon* **2018**, *132*, 556.
- [10] a) P. Ouzilleau, A. E. Gheribi, P. Chartrand, *Carbon* **2016**, *109*, 896; b) P. J. F. Harris, *Crit. Rev. Solid State* **2005**, *30*, 235.
- [11] a) B. E. Barton, M. J. Behr, J. T. Patton, E. J. Hukkanen, B. G. Landes, W. Wang, N. Horstman, J. E. Rix, D. Keane, S. Weigand, M. Spalding, C. Derstine, *Small* **2017**, *13*; b) H. Wang, Q. Guo, J. Yang, Z. Liu, Y. Zhao, J. Li, Z. Feng, L. Liu, *Carbon* **2013**, *56*, 296.
- [12] a) Z. Gao, J. Zhu, S. Rajabpour, K. Joshi, M. Kowalik, B. Croom, Y. Schwab, L. Zhang, C. Bumgardner, K. R. Brown, D. Burden, J. W. Klett, A. C. T. van Duin, L. V. Zhigilei, X. Li, C. V. A. Univ. of Virginia, *Sci. Adv.* **2020**, *6*, eaaz4191; b) S. Zhang, Y. Ma, L. Suresh, A. Hao, M. Bick, S. C. Tan, J. Chen, *ACS Nano* **2020**, *14*, 9282; c) D. Papkov, A. Goponenko, O. C. Compton, Z. An, A. Moravsky, X.-Z. Li, S. T. Nguyen, Y. A. Dzenis, *Adv. Funct. Mater.* **2013**, *23*, 5763; d) W. Eom, S. H. Lee, H. Shin, W. Jeong, K. H. Koh, T. H. Han, *ACS Nano* **2021**, *15*, 13055.
- [13] E. S. Penev, V. I. Artyukhov, B. I. Yakobson, *Carbon* **2015**, *85*, 72.

- [14] Z. Xu, Y. Liu, X. Zhao, L. Peng, H. Sun, Y. Xu, X. Ren, C. Jin, P. Xu, M. Wang, C. Gao, *Adv. Mater.* **2016**, *28*, 6449.
- [15] a) M. B. Vázquez-Santos, E. Geissler, K. László, J.-N. Rouzaud, A. Martínez-Alonso, J. M. D. Tascón, *J. Phys. Chem. C* **2011**, *116*, 257; b) L. G. Cançado, K. Takai, T. Enoki, M. Endo, Y. A. Kim, H. Mizusaki, A. Jorio, L. N. Coelho, R. Magalhães-Paniago, M. A. Pimenta, *Appl. Phys. Lett.* **2006**, *88*, 163106.
- [16] a) L. Peng, Y. Han, M. Wang, X. Cao, J. Gao, Y. Liu, X. Chen, B. Wang, B. Wang, C. Zhu, X. Wang, K. Cao, M. Huang, B. V. Cunnings, J. Pang, W. Xu, Y. Ying, Z. Xu, W. Fang, Y. Lu, R. S. Ruoff, C. Gao, *Adv. Mater.* **2021**, *33*, 2104195; b) H. Huang, X. Ming, Y. Wang, F. Guo, Y. Liu, Z. Xu, L. Peng, C. Gao, *Carbon* **2021**, *180*, 197; c) M. Huang, P. V. Bakharev, Z. J. Wang, M. Biswal, Z. Yang, S. Jin, B. Wang, H. J. Park, Y. Li, D. Qu, Y. Kwon, X. Chen, S. H. Lee, M. G. Willinger, W. J. Yoo, Z. Lee, R. S. Ruoff, *Nat. Nanotechnol.* **2020**, *15*, 289.
- [17] a) C. Zhao, P. Zhang, J. Zhou, S. Qi, Y. Yamauchi, R. Shi, R. Fang, Y. Ishida, S. Wang, A. P. Tomsia, M. Liu, L. Jiang, *Nature* **2020**, *580*, 210; b) J. Huang, J. Zhou, M. Liu, *JACS Au* **2022**, *2*, 280.
- [18] C. Pramanik, T. Jamil, J. R. Gissinger, D. Guittet, P. J. Arias-Monje, S. Kumar, H. Heinz, *Adv. Funct. Mater.* **2019**, *29*, 1905247.
- [19] J. Meng, Y. Zhang, S. W. Cranford, M. L. Minus, *J. Phys. Chem. B* **2014**, *118*, 9476.
- [20] a) W. J. W Watt, *Nature* **1975**, *257*, 210; b) M. S. A. Rahaman, A. F. Ismail, A. Mustafa, *Polym. Degrad. Stab.* **2007**, *92*, 1421.
- [21] a) Y. Liu, S. Kumar, *Polymer Reviews* **2012**, *52*, 234; b) E. Fitzer, W. Frohs, M. Heine, *Carbon* **1986**, *24*, 387; c) M. Ji, C. Wang, Y. Bai, M. Yu, Y. Wang, *Polymer Bulletin* **2007**, *59*, 527.
- [22] a) N. V. Salim, X. Jin, J. M. Razal, *Compos. Sci. Technol.* **2019**, *182*, 107781; b) I. Gergin, E. Ismar, A. S. Sarac, *Beilstein J. Nanotechnol.* **2017**, *8*, 1616; c) K. Wang, M. Li, J. Zhang, H. Lu, *Carbon* **2019**, *144*, 249.
- [23] a) Y. Cheng, G. Cui, C. Liu, Z. Liu, L. Yan, B. Liu, H. Yuan, P. Shi, J. Jiang, K. Huang, K. Wang, S. Cheng, J. Li, P. Gao, X. Zhang, Y. Qi, Z. Liu, *Adv. Funct. Mater.* **2021**, *32*, 2103493; b) G. Xin, W. Zhu, Y. Deng, J. Cheng, L. T. Zhang, A. J. Chung, S. De, J. Lian, *Nat. Nanotechnol.* **2019**, *14*, 168.
- [24] H. Park, K. H. Lee, Y. B. Kim, S. B. Ambade, S. H. Noh, W. Eom, J. Y. Hwang, W. J. Lee, J. Huang, T. H. Han, *Sci. Adv.* **2018**, *4*, eaau2104.
- [25] Y. Liu, P. Li, F. Wang, W. Fang, Z. Xu, W. Gao, C. Gao, *Carbon* **2019**, *155*, 462.
- [26] M. Kowalik, C. Ashraf, B. Damirchi, D. Akbarian, S. Rajabpour, A. C. T. van Duin, *J. Phys. Chem. B* **2019**, *123*, 5357.
- [27] a) S. Rajabpour, Q. Mao, Z. Gao, M. Khajeh Talkhonch, J. Zhu, Y. Schwab, M. Kowalik, X. Li, A. C. T. van Duin, *Carbon* **2021**, *174*, 345; b) H. G. Chae, M. L. Minus, A. Rasheed, S. Kumar, *Polymer* **2007**, *48*, 3781; c) Y. Liu, H. G. Chae, S. Kumar, *Carbon* **2011**, *49*, 4466.

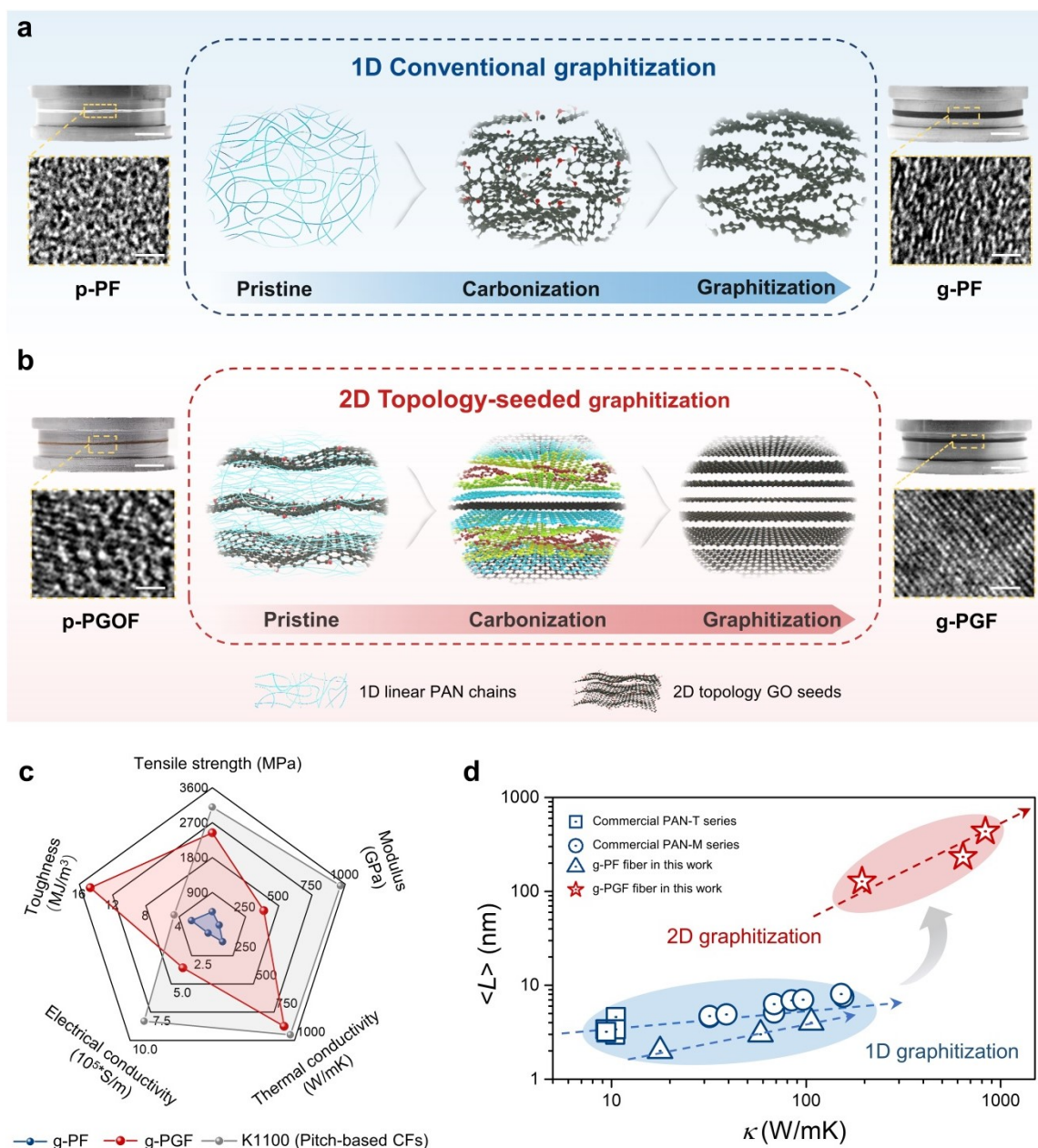


Figure 1. a) Schematic illustration of internal graphitic crystal structure via 1D conventional graphitization route. Corresponding optical and HR-TEM images of p-PF and g-PF on the graphite reels show similarly disordered texture. b) Schematic illustration of internal graphitic crystal structure via 2D topology-seeded graphitization strategy. Corresponding optical and HR-TEM images of p-PGOF (30% GO seeds) and g-PGF (30% GO seeds) on the graphite reels show high crystallinity. c) Overall mechanical and conductive performances of CFs with 2D topology-seeded graphitization strategy (g-PGF, red line), pure PAN-based CFs (g-PF, blue line) and the best Pitch-based CFs (K1100, gray line)^[4a]. d) Thermal conductivity

versus the crystal size for PGF and other conventional PAN-based CFs^[5b]. Scale bar, 10 mm for digital images and 2 nm for HR-TEM images (a, b).

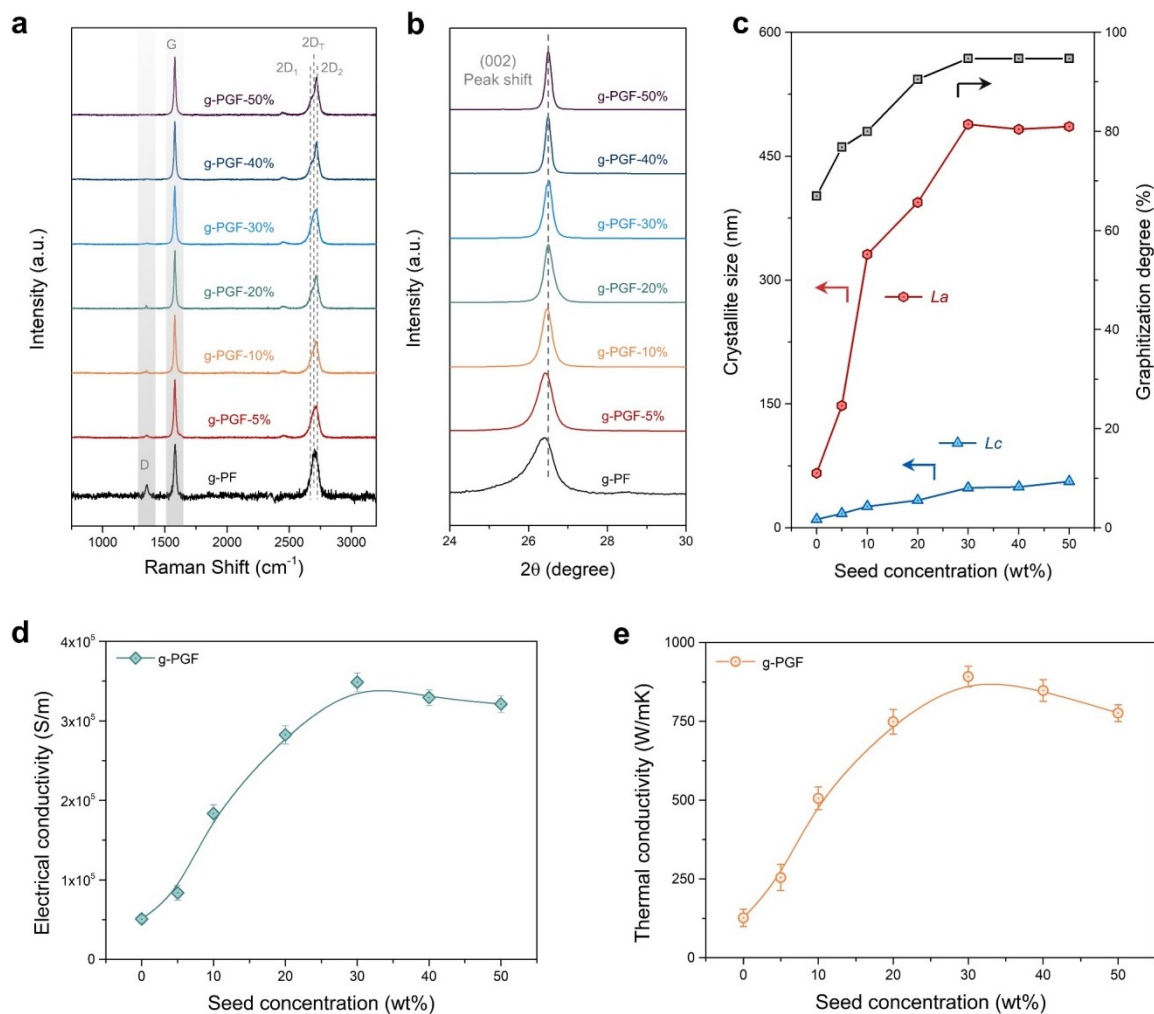


Figure 2. a) Raman spectra of the g-PF and g-PGFs with varied GO seed concentrations after graphitization at 3000 °C. Raman spectra were obtained over the range 800-3500 cm⁻¹ under ambient condition using an excitation wavelength of 532 nm laser beam. The 2D peak is fitted with 3 Lorentzian peaks: 2D¹ (~2680 cm⁻¹) and 2D² (~2720 cm⁻¹) for AB stacked graphite and 2D^T (~2700 cm⁻¹) for turbostratic graphite crystal structure. b) XRD profiles of g-PF and g-PGF with varied GO seed concentrations after graphitization at 3000 °C. c) Crystallite sizes (*L_a* and *L_c*) and graphitization degrees of g-PF and g-PGF with varied GO seed concentrations after graphitization at 3000 °C. The *L_a* of fibers is calculated from the Raman spectra. The *L_c* and graphitization degrees of fibers are obtained from the XRD (002) peak profiles. d) and e) Thermal and electrical conductivities of g-PF and g-PGF with varied GO seed concentrations after graphitization at 3000 °C.

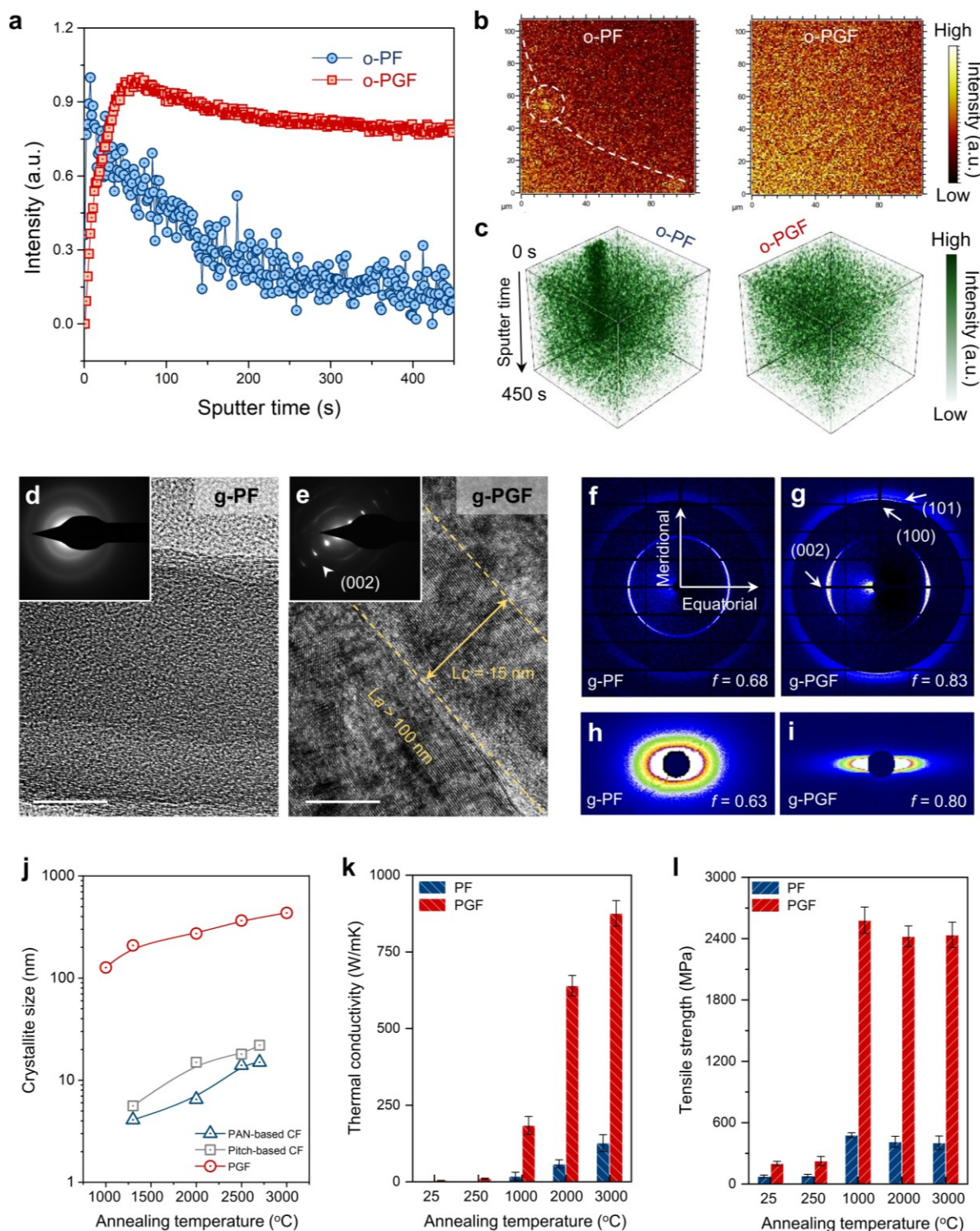


Figure 3. a) TOF-SIMS depth profiles of O element in the o-PF and o-PGF (30% GO seeds) after oxidation. b) 2D mappings of ToF SIMS O element on the surface of the o-PF and o-PGF (30% GO seeds) after oxidation process. The white dotted line in the o-PF indicated the nonuniformed distribution of O element. c) Corresponding 3D rendering of O- secondary ion distribution from surface to internal parts of o-PF and o-PGF (30% GO seeds). d) HR-TEM

image of the g-PF and the corresponding selected area electron diffraction patterns (inset shows SAED). e) HR-TEM image of the g-PGF (30% GO seeds) and the corresponding selected area electron diffraction patterns (inset shows SAED). f-i) 2D WAXS patterns and SAXS patterns of the g-PF and g-PGF (30% GO seeds). The f in WAXS is calculated from (002) peak. j) Crystallite sizes (L_a) as a function of annealing temperature in PGF, PAN-based CFs and Pitch-based CFs, respectively. The L_a values of commercial PAN-based CFs and Pitch-based CFs are obtained from XRD^[5b]. The L_a values of graphited PGF (30% GO seeds) are obtained from Raman. k, l) Thermal conductivity (k) and tensile strength (l) of PF and PGF (30% GO seeds) annealed at different heat-treatment stages. Scale bar: 10 nm (e, d).

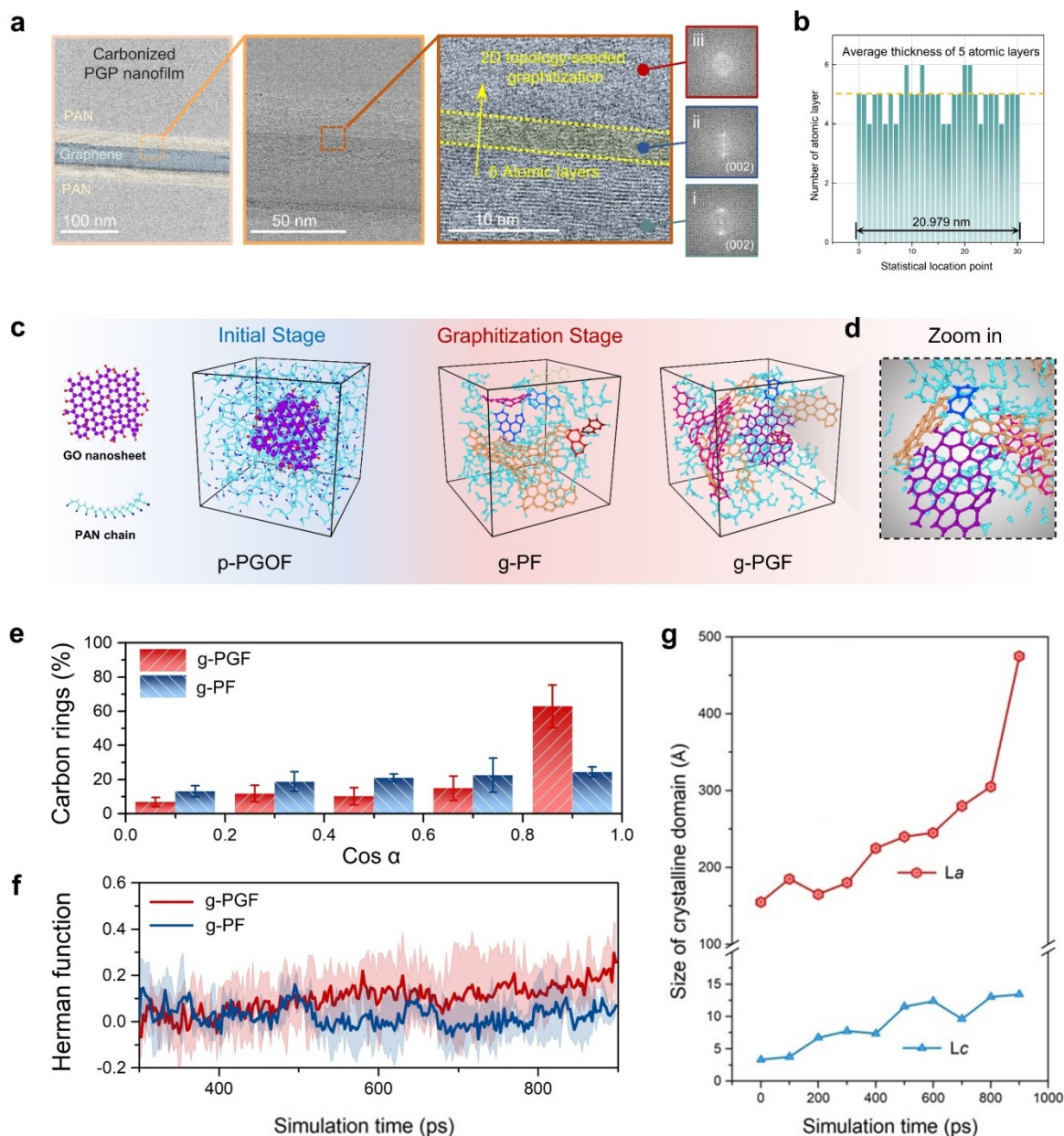


Figure 4. a) Cross-sectional HR-TEM images of c-PGP composite nanofilm after annealed at 1000 °C. The corresponding FFT images in different graphite crystallite domains. b) Average statistics of atomic layers via 2D topology-seeded graphitization. c) Atomistic ReaxFF simulations of the initial stage and graphitization process for PF and PGOF (30% GO seeds). d) Snapshots of the PGOF taken during the graphitization process to show carbon layer structures near the initial 2D GO seed. Purple spheres represent the initial graphene structure. Red, green and yellow spheres are represented newly formed graphene-like layers, respectively. e) Orientation distributions of carbon rings in g-PF and g-PGF after graphitization. f) Herman functions of g-PF and g-PGOF at different simulation times. All curves represent the average values over 3 samples and the shadow areas represent the

corresponding standard deviations. g) Size of graphite crystalline domains in the g-PGF at different simulation times.

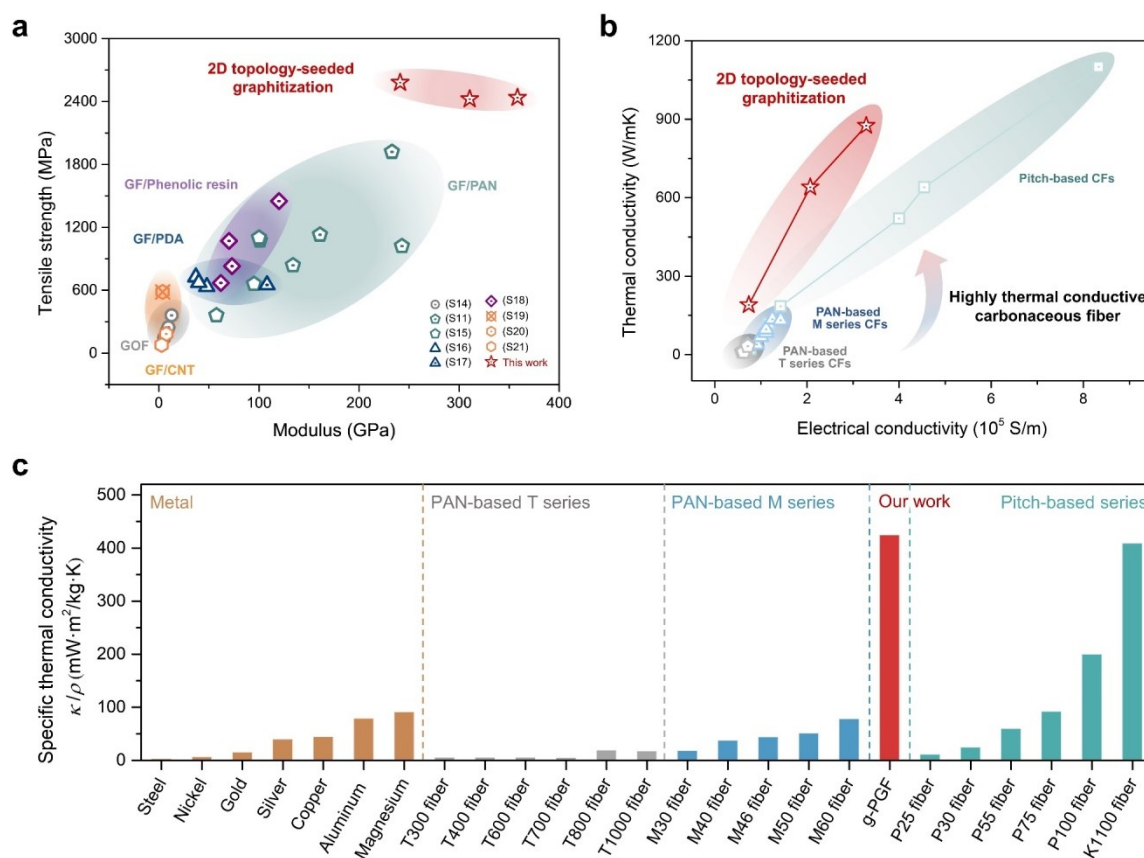


Figure 5. a) Ashby plot of tensile strength versus Young's modulus of PGF, PAN-based CFs, Pitch-based CFs and other GO/polymer composited CFs. b) Ashby plot of thermal conductivity versus electrical conductivity of g-PGF (30% GO seeds), PAN-based CFs and Pitch-based CFs^[2a, 4a, 5b, 6b]. The thermal conductivity and electrical conductivity of g-PGF (30% GO seeds) are measured through the steady-state electrical heating method and the standard four-probe method. c) Comparison of the specific thermal conductivity of the g-PGF (30% GO seeds) with other metal fibers, PAN-based CFs and Pitch-based CFs^[1c, 2a, 4a].

ToC of the manuscript

2D topology-seeded graphitization strategy effectively generate a new species of highly thermally conductive carbon fibers. Strong mechanical strength and high thermal conductivity up to 850 W/mK are simultaneously realized, which is one order of magnitude more conductive than commercial PAN-based carbon fibers. These fibers have great potential for lightweight thermal management materials, high-power electronics and energy storage.

Xing Ming, Anran Wei, Yingjun Liu, Li Peng, Peng Li, Jiaqing Wang, Sengping Liu, Wenzhang Fang, Ziqiu Wang, Huanqin Peng, Jiahao Lin, Haoguang Huang, Zhanpo Han, Shiyu Luo, Min Cao, Bo Wang, Zheng Liu, Fenglin Guo^{}, Zhen Xu^{*}, Chao Gao^{*}*

Two-dimensional Topology-Seeded Graphitization for Highly Thermally Conductive Carbon Fibers